

Uncertainty on w from large-scale structure

Valerio Marra¹, Mikko Pääkkönen^{2,3} and Wessel Valkenburg^{1,4}

¹*Institut für Theoretische Physik, Universität Heidelberg, Philosophenweg 16, 69120 Heidelberg, Germany*

²*Department of Physics, PL 35, 40014 University of Jyväskylä, Finland*

³*Helsinki Institute of Physics, PL 64, 00014 University of Helsinki, Finland*

⁴*Instituut-Lorentz for Theoretical Physics, Universiteit Leiden, Postbus 9506, 2333 CA Leiden, The Netherlands*

Accepted XXX. Received XXX; in original form XXX

ABSTRACT

We find that if we live at the center of an inhomogeneity with total density contrast $|\delta_0| \simeq 0.1 - 0.15$, dark energy is *not* a cosmological constant at 95% confidence level. Observational constraints on the equation of state of dark energy, w , depend strongly on the local matter density around the observer. We model the local inhomogeneity with an exact spherically symmetric solution which features a pressureless matter component and a dark-energy fluid with constant equation of state and negligible sound speed, that reaches a homogeneous solution at finite radius. We fit this model to observations of the local expansion rate, distant supernovae and the cosmic microwave background. We conclude that the possible uncertainty from large-scale structure has to be taken into account if one wants to progress towards not just precision but also accurate cosmology.

Key words: cosmological parameters – large-scale structure of Universe – cosmology: observations

1 INTRODUCTION

We have entered the so-called era of accurate cosmology (Peebles 2002). The aim is to understand the composition and expansion history of the universe at the percent level. In particular, one of the goals is to establish if the observed acceleration of the universe (Perlmutter et al. 1999; Riess et al. 1998) is driven by the cosmological constant or by a fluid with negative pressure, dark energy. At the most basic level the question is if the observed equation of state w is compatible with -1 or not, the value corresponding to the cosmological constant. It is therefore crucial to study all possible systematic effects on w (Amendola et al. 2010; Sinclair et al. 2010; Marra & Paakkonen 2010; de Lavallaz & Fairbairn 2011; Romano & Chen 2011).

As our observations are confined to the light cone, there is an intrinsic degeneracy between temporal evolution and spatial variation around us. In particular, inhomogeneities around us are degenerate with the properties of dark energy, most importantly its equation of state. A clear example of how intertwined are attempts to detect any evolution of dark energy to large-scale structures is given by the so-called “void models”. An observer inside a spherical underdensity expanding faster than the background sees indeed apparent acceleration, thus removing the need for dark energy (see e.g. Marra & Notari 2011, and references therein). Void models strongly violate the Copernican principle and have been ruled out – at least in their simplest incarnation – as they predict a too strong kinematic Sunyaev-Zel’Dovich ef-

fect (Garcia-Bellido & Haugboelle 2008; Zhang & Stebbins 2011; Zibin & Moss 2011; Zibin 2011). While on one hand this strengthens the case for dark energy as the likely explanation for the acceleration of the universe, on the other hand it illustrates how large-scale structure can alter the determination of cosmological parameters. Therefore, it is necessary to adequately model large-scale structures if one has to achieve the grand goal of accurately determining the composition of the universe.

In Valkenburg (2012b) it was shown by means of mock data that a local inhomogeneity, of proportions similar to a structure on the surface of last scattering that could cause the CMB Cold Spot, can have strong effects on our perception of the equation of state of dark energy. Here we extend that analysis to real data using the model of Marra & Paakkonen (2012). More precisely, we consider a w CDM model endowed with a local almost-linear inhomogeneity surrounding the observer and test it against supernova observations, CMB anisotropies and local measurements of the Hubble parameter. By w CDM we mean a universe containing dark matter and a dark-energy fluid with equation of state w . In this way we can show how the observed large-scale structure of the universe could impact the reconstruction of the dark-energy parameters.

Following Valkenburg (2012b), we consider an inhomogeneity inspired by the observed Cold Spot in the CMB, which has a radius of roughly 5° and a temperature devia-

tion of roughly $\mathcal{O}(50 \sim 200) \mu\text{K}$.¹ The idea is that the Cold Spot is a primary CMB anisotropy due to an object on the surface of last scattering, and not a secondary effect caused by an object along the line of sight (Tomita 2005; Inoue & Silk 2006, 2007; Masina & Notari 2009). Such an inhomogeneity has a radius of roughly 1 Gpc and a density contrast today of roughly -0.1 (Valkenburg 2012b). It is therefore too shallow to bias the w CDM model to the point of removing the need for dark energy, as in the void scenario. Nonetheless, as argued above, such a structure may bias the value of the dark-energy parameters to a level that may be important if one wants to determine whether dark energy is a cosmological constant or not. Moreover, as we briefly argue in the body of this paper, structures of radius ~ 1 Gpc and density contrast today ~ 0.01 – which still give an interesting effect – are not at more than three times the dispersion of the density perturbations arising from a close to scale-invariant primordial spectrum. Therefore, the setup considered in this paper is not in conflict with standard cosmology and, in particular, the Copernican principle (Valkenburg et al. 2012).

We model the inhomogeneity with a particular case of the spherically symmetric solution presented in Marra & Paakkonen (2012), which features a pressureless matter component and a dark-energy fluid with constant equation of state and negligible sound speed c_s . The possibility of a dark-energy fluid with negligible sound speed has been investigated in the literature under various assumptions. This generally requires a non canonical scalar field like k -essence and kinetic gravity braiding, as opposed to standard quintessence models with canonical scalar fields which always have $c_s = 1$ (see e.g. Creminelli et al. 2009; Bertacca et al. 2008; Lim et al. 2010; Bertacca et al. 2010; Defay et al. 2010; Li et al. 2011, and references therein). Here we choose this particular model because it significantly simplifies the dynamical equations and the numerical analysis as there are no pressure gradients that can generate peculiar velocities from an initially comoving motion. We use this model phenomenologically so as to minimally extend the parameter space of the w CDM model by adding only two extra parameters: the radius of the inhomogeneity and its overall contrast. All the other initial conditions follow indeed rigidly.

The paper is organized as follows. In Section 2 we go briefly through the formalism of the model and its initial conditions, and in Section 3 we explain how the cosmological data analysis has been performed. We show in Section 4 that the effect of local inhomogeneity on the dark-energy parameters can be important and that the inhomogeneity is not unlikely to occur. We conclude in Section 5.

2 THE MODEL

We consider the case of an observer located at the center of an inhomogeneous sphere embedded in a flat w CDM universe. The inhomogeneities are given by a pressureless matter component and by a dark-energy fluid with constant

equation of state w_{out} and negligible sound speed (the subscript “out” refers to values at $r > r_b$ where r_b is the comoving radius of the inhomogeneity). To be more precise, the sound horizon is much smaller than the inhomogeneity scale considered so that we can set $c_s = 0$ throughout the paper. In terms of the radius dependent non-adiabatic equation of state this means that we consider:

$$w(r, t) = w_{\text{out}} \frac{\rho_{X,\text{out}}(t)}{\rho_X(r, t)}, \quad (1)$$

that is, the pressure is homogenous:

$$p_X(r, t) = p_{X,\text{out}}(t) = w_{\text{out}} \rho_{X,\text{out}}(t), \quad (2)$$

where r is the coordinate radius, t is cosmic time, ρ denotes energy density, p denotes pressure and the label X refers to the dark-energy fluid. Since pressure gradients are absent, matter and dark energy evolve along geodesics. Moreover, we set initial conditions such that dust and dark energy are initially comoving. Therefore, the absence of pressure gradients implies that peculiar velocities between the two fluids will never develop and that the matter and dark-energy reference frames always coincide. Next, we discuss the equations governing the dynamics of the model and the relevant initial conditions.

2.1 Dynamical equations

We adopt the exact spherically symmetric inhomogeneous solution with n perfect fluids presented in Marra & Paakkonen (2012), which we limit to the case discussed above. We will now briefly introduce the relevant equations, and we refer to Marra & Paakkonen (2012) for the general equations and more details.

Using the reference frame of the dust and dark-energy components, the metric describing our model is:

$$ds^2 = -dt^2 + \frac{Y'(r, t)^2}{1 - k(r)r^2} dr^2 + Y(r, t)^2 d\Omega^2, \quad (3)$$

where $Y(r, t)$ is the scale function, $k(r)$ is the curvature function, $d\Omega^2 = d\theta^2 + \sin^2 \theta d\phi^2$ and we have set $c = 1$. A prime denotes partial derivation with respect to the coordinate radius r , whereas a dot denotes partial derivation with respect to the coordinate time t . The curvature function is time independent because of the adopted reference frame and sound speed (Marra & Paakkonen 2012). The metric (3) is written in the same form as the Lemaître-Tolman-Bondi (LTB) metric. However, with the inclusion of a dark-energy fluid, the dynamics is no longer that of the LTB metric. The metric of Eq. (3) reduces to the Friedman-Lemaître-Robertson-Walker (FLRW) metric if $k(r) = \text{const}$ and $Y(r, t) = r a(t)$, where $a(t)$ is the scale factor.

We label the dust component with M and the dark-energy component with X . The conservation equation for the dust source can be solved directly and gives:

$$\frac{\rho_M(r, t)}{\rho_M(r, \bar{t})} = \frac{Y^2(r, \bar{t})Y'(r, \bar{t})}{Y^2(r, t)Y'(r, t)}, \quad (4)$$

where \bar{t} is the initial time at which we give the initial conditions. As explained before, there are no peculiar velocities

¹ See e.g. Cruz et al. (2006); Zhang & Huterer (2010); Bennett et al. (2011).

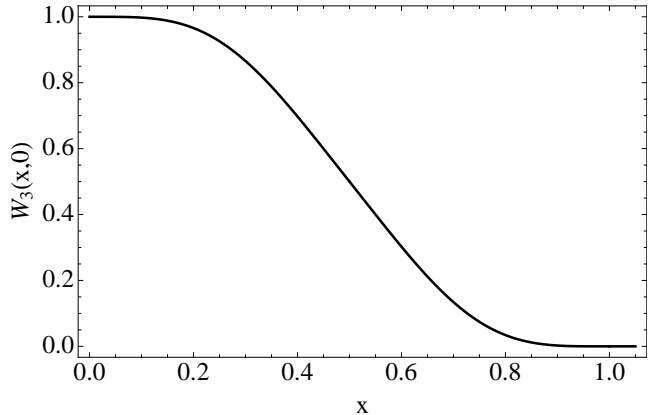


Figure 1. Shape of the auxiliary function $W_3(x, 0)$ that is used in Eq. (11) to model the curvature profile.

between the two fluids and the remaining dynamical equations reduce to:

$$\dot{Y}^2(r, t) = \frac{2GF(r, t)}{Y(r, t)} - k(r)r^2, \quad (5)$$

$$\dot{Y}'(r, t) = \frac{GF'(r, t)}{Y(r, t)\dot{Y}(r, t)} - \frac{GF(r, t)Y'(r, t)}{Y^2(r, t)\dot{Y}(r, t)} - \frac{[k(r)r^2]'}{2\dot{Y}(r, t)}, \quad (6)$$

$$\dot{F}(r, t) = -4\pi Y^2(r, t)\dot{Y}(r, t)p_{X, \text{out}}(t), \quad (7)$$

$$\dot{\rho}_X(r, t) = -\left[\rho_X(r, t) + p_{X, \text{out}}(t)\right]\left[H_R(r, t) + 2H_A(r, t)\right], \quad (8)$$

where the radial and angular expansion rates are $H_R = \dot{Y}'/Y'$ and $H_A = \dot{Y}/Y$, and F is the total effective gravitating mass which also satisfies the following consistency equation:

$$F'(r, t) = 4\pi Y^2(r, t)Y'(r, t)\left[\rho_M(r, t) + \rho_X(r, t)\right]. \quad (9)$$

Eq. (6) is the r -derivative of Eq. (5) and allows us to solve directly for the unknown functions Y , Y' , F and ρ_X without having to take numerical derivatives. If $w = w_{\text{out}} = -1$, this solution becomes the usual ALTB model which has been studied recently in, e.g., [Enqvist & Mattsson \(2007\)](#); [Sinclair et al. \(2010\)](#); [Marra & Paakkonen \(2010\)](#); [Valkenburg \(2012a\)](#); [Romano & Chen \(2011\)](#).

Finally, in this particular case the light-cone equations have the same form as in the LTb model:

$$\frac{dt}{dz} = -\frac{Y'}{(1+z)\dot{Y}'}, \quad \frac{dr}{dz} = \frac{\sqrt{1-k(r)r^2}}{(1+z)\dot{Y}'}. \quad (10)$$

2.2 Initial and boundary conditions

We fix the flat w CDM background model by setting h , Ω_X and w_{out} , where Ω_X is the present-day background dark-energy density parameter and h is the present-day dimensionless Hubble rate defined by $H_0 = 100 h \text{ km s}^{-1} \text{ Mpc}^{-1}$.

We fix the gauge for the radial coordinate in Eq. (3) such that $Y(r, \bar{t}) = r a(\bar{t})$ at some initial time \bar{t} . We choose to parametrize the curvature by means of

$$k(r) = k_c W_3\left(\frac{r}{r_b}, 0\right), \quad (11)$$

where r_b is the comoving radius of the spherical inhomogeneity and:

$$W_3(x, 0) = \begin{cases} \frac{1}{4\pi^2} + 1 - 2x^2 - \frac{\cos(4\pi x)}{4\pi^2} & \text{for } 0 \leq x < \frac{1}{2} \\ \frac{-1}{4\pi^2} + 2(1-x)^2 + \frac{\cos(4\pi x)}{4\pi^2} & \text{for } \frac{1}{2} \leq x < 1, \\ 0 & \text{for } x \geq 1 \end{cases} \quad (12)$$

is the third order of the function $W_n(x, \alpha)$, which has been defined in [Valkenburg \(2012a\)](#) and interpolates from 1 to 0 in the interval $\alpha < x < 1$ while remaining C^n everywhere. Hence $k(r)$ is C^3 everywhere, such that the metric is C^2 and the Riemann curvature is C^0 . Although the function $W_3(x, 0)$ looks rather complicated, it has actually a very simple shape as one can see in Fig. 1. The curvature profile of Eq. (11) is exactly zero for $r \geq r_b$ and so the metric is correctly matched to the exterior spatially-flat w CDM model, which means that the central over- or under-density is automatically compensated by a surrounding under- or over-dense shell. The constant k_c gives the curvature at the center of the inhomogeneity and will determine its density contrast. A spherical inhomogeneity depends crucially on only two *physical* parameters: the radius and the overall density contrast. Therefore, the precise shape of the density profile should not be essential and our analysis should be representative also of other possible curvature or density profiles.

Next, we have to give initial conditions at $t = \bar{t}$ for $F(r, \bar{t}) = \bar{F}_M(r) + \bar{F}_X(r)$. We choose \bar{t} such that matter is dominant over dark energy, $\bar{F}_X(r) \ll \bar{F}_M(r)$, and so the model becomes the standard dust LTb model. We can then link the curvature function $k(r)$ to the initial condition for $\bar{F}_M(r)$ by demanding that the universe has the same age \bar{t} for any r . That is, we demand a homogeneous Big Bang, implying the absence of decaying modes in the matter density ([Zibin 2008](#)). In particular we can use the following analytic result of [Van Acoleyen \(2008\)](#) valid for a linear matter density contrast:

$$k(r) \simeq \frac{5}{3} a^2(\bar{t}) H_{\text{out}}(\bar{t})^2 \bar{\delta}_{F_M}(r), \quad (13)$$

which clearly relates the curvature at the center k_c to the matter contrast at the center $\bar{\delta}_M = \bar{\delta}_{F_M}(0)$. The latter term is the contrast in the gravitating mass and is defined as:

$$\bar{\delta}_{F_M}(r) = \frac{\bar{F}_M(r)}{\bar{F}_{M, \text{out}}(r)} - 1, \quad (14)$$

where $\bar{F}_{M, \text{out}} = \frac{4\pi}{3} a^3(\bar{t}) r^3 \rho_{M, \text{out}}(\bar{t})$ is the corresponding background gravitating mass and the gauge $Y(r, \bar{t}) = r a(\bar{t})$ has been used. The initial matter density is then:

$$\rho_M(r, \bar{t}) = \frac{\bar{F}'_M(r)}{4\pi a^3(\bar{t}) r^2}. \quad (15)$$

In order to have initial conditions without decaying modes in the dark-energy component, we have to set its initial profile according to the following relation valid during matter domination and $c_s^2 \ll 1$ ([Ballesteros & Lesgourgues 2010](#)):

$$\frac{\bar{\delta}_{F_X}(r)}{\bar{\delta}_{F_M}(r)} = \frac{\bar{\delta}_X}{\bar{\delta}_M} = \frac{1 + w_{\text{out}}}{1 - 3w_{\text{out}}}, \quad (16)$$

where, analogous to the matter contrast, we have,

$$\bar{\delta}_{F_X}(r) = \frac{\bar{F}_X(r)}{\bar{F}_{X,\text{out}}(r)} - 1, \quad (17)$$

$\bar{F}_{X,\text{out}} = \frac{4\pi}{3} a^3(\bar{t}) r^3 \rho_{X,\text{out}}(\bar{t})$ and $\bar{\delta}_X = \bar{\delta}_{F_X}(0)$. The initial dark-energy density is then,

$$\rho_X(r, \bar{t}) = \frac{\bar{F}'_X(r)}{4\pi a^3(\bar{t}) r^2}. \quad (18)$$

Hence, all the initial conditions relative to the inhomogeneous patch are indeed specified by a given curvature profile $k(r)$.

3 COSMOLOGICAL DATA ANALYSIS

In this Section we explain how we compare the predictions of this model with supernovae, Hubble rate and cosmic microwave background observations. We decided not to include baryon acoustic oscillations in the analysis as perturbation theory in an inhomogeneous background has not been thoroughly understood yet² (Zibin 2008; Clarkson et al. 2009; Alonso et al. 2010).

3.1 Hubble rate

The Hubble rate is obtained by measuring cosmological standard candles mostly within a redshift range with median value $z_h \sim 0.05$. We compare the observed value to the theoretical quantity,

$$H_{\text{loc}} = \frac{1}{z_{\text{max}} - z_{\text{min}}} \int_{z_{\text{min}}}^{z_{\text{max}}} H_A(r(z), t(z)) dz. \quad (19)$$

The values z_{max} and z_{min} depend on the redshift volume that is probed by a given experiment. The reason we compare an averaged expansion rate to the data is primarily because the observed expansions rate in fact is an averaged quantity, so this should be a fair comparison. Moreover, when the redshift z_b of the boundary of the inhomogeneity is close in value to z_h , the averaged H_{loc} may differ significantly from $H_A(r(z_h), t(z_h))$, which falsely would lead to a bad fit. The approach of Eq. (19) is to some extent arbitrary and one should instead reanalyze the raw data without assuming a FLRW fiducial model as it is usually done (see e.g. the discussion in Zumalacarregui et al. 2012). However, as we will see in Section 3.3 our results depend weakly on the Hubble parameter constraint and so this caveat should not sizably affect our findings.

We mainly consider the determination of the Hubble rate from Riess et al. 2009 (R09). However, in order to study a possible sensitive dependence on this datum, we will also consider the results from Freedman et al. 2001 (F01) and Sandage et al. 2006 (S06). The three measurements are:

$$H_{F01} = 72 \pm 8 \frac{\text{km/s}}{\text{Mpc}}, \quad 0.005 < z < 0.1, \quad (20)$$

$$H_{S06} = 62.3 \pm 6.3 \frac{\text{km/s}}{\text{Mpc}}, \quad 0.01 < z < 0.07, \quad (21)$$

$$H_{R09} = 74.2 \pm 3.6 \frac{\text{km/s}}{\text{Mpc}}, \quad 0.023 < z < 0.1. \quad (22)$$

² See, however, Nishikawa et al. (2012) for a recent development.

3.2 Supernova observations

We use the Union2 SN Compilation (Amanullah et al. 2010), which consists of 557 type Ia supernovae in the redshift range $z = 0.015 - 1.4$. As we are considering an almost-linear inhomogeneity surrounding the observer, we are not departing strongly from the standard model. Therefore it should be a good approximation to use the magnitude-redshift and correlation tables provided by Amanullah et al. (2010).

3.3 Cosmic microwave background

The metric of Eq. (3) is matched to the background FLRW metric at a redshift at which radiation is still negligible. In this way the last scattering surface, which is responsible for most of the CMB anisotropies, is outside the inhomogeneous patch and a standard analysis of the primordial CMB power spectrum is possible. One has to replace the inhomogeneous model with an *effective* FLRW metric which accounts for the different angular diameter distance to the surface of last scattering of the CMB as compared to the homogeneous background model. This is done by placing an FLRW observer ($\delta_0 \equiv 0$) in the same coordinate system at $r = 0$ but at a different time than t_0 , such that this observer's angular diameter distance to the surface of last scattering, which lies at some constant time t_{LS} , agrees with the actual LTB observer's angular diameter distance to the surface of last scattering. The physics at last scattering itself is unaffected, since the *effective* FLRW observer is placed in the same FLRW universe in which the LTB patch is embedded, albeit at a different time. The CMB spectrum is then calculated using CAMB (Lewis et al. 2000). See Biswas et al. (2010); Moss et al. (2011); Marra & Paakkonen (2010) for more explicit details about how the effective model is obtained. Note that there are other contributions to the CMB coming from secondary effects, which in the inhomogeneity may differ from those in the effective FLRW metric, and are due to the photons traveling through inhomogeneities inside the void, such as the late-time ISW effect and weak lensing. For the same reason as for which we ignore the baryon acoustic oscillations, we ignore these secondary effects, since they are subdominant and studying them would require knowledge of the growth of perturbations in an inhomogeneous background. We fit the theoretical predictions of our model to the WMAP 7-year data release (Komatsu et al. 2011).

3.4 Parameter estimation

We perform a Markov-Chain Monte-Carlo likelihood analysis using COSMOMC (Lewis & Bridle 2002). We calculate all distance measures using an improved version of VOID-DISTANCESII³ (Biswas et al. 2010), which now acts as a wrapper around CAMB (Lewis et al. 2000), necessitating no changes to CAMB's source code and minimal changes to COSMOMC's source code. We combine this module with the ALTB module COLLAMBDA⁴ (Valkenburg 2012a) for calculating all metric functions, which we extended to include

³ <http://web.physik.rwth-aachen.de/download/valkenburg/>

⁴ <http://web.physik.rwth-aachen.de/download/valkenburg/CollLambda/>

Flat priors			
0.4	<	h	< 1
0.005	<	$\Omega_b h^2$	< 0.1
0.001	<	$\Omega_{\text{dm}} h^2$	< 0.99
-2	<	w_{out}	< -0.4
0.01	<	τ	< 0.8
2.7	<	$\log 10^{10} A_S$	< 4
0.5	<	n_S	< 1.5
-0.2	<	α_S	< 0.2
-0.2	<	δ_0	< 0.2
100 Mpc	<	$d(r_b)$	< 3 Gpc
Additional constraints			
Ω_X	>	0	
Ω_k	=	0	

Table 1. Priors imposed on the parameters in the numerical analysis. The size of the LTB patch $d(r_b)$ is defined in Eq. (23). The additional constraint $\Omega_X > 0$ with $\Omega_k = 0$, in fact implies a non-flat prior on both $\Omega_{\text{dm}} h^2$ and h , as explained in Appendix A.

the numerical solutions to the scenario discussed here, with $w_{\text{out}} \neq -1$ and $c_s = 0$. With this setup, for every selected vector of parameter values, we calculate the theoretical predictions for supernova distances, the local Hubble rate and the CMB power spectrum. For reference, next to the inhomogeneous model we analyze its homogeneous background model, $w\text{CDM}$, which is described by the same model but has $z_b \equiv 0$ and $\delta_0 \equiv 0$.

We take flat priors on the parameters listed in Table 1. Most of these are the usual cosmological parameters: the background present-day Hubble rate h , the background baryon density $\Omega_b h^2$, the background dark-matter density $\Omega_{\text{dm}} h^2$, the equation of state of dark energy w_{out} , the optical depth to re-ionization τ , the amplitude of primordial scalar perturbations A_S , the tilt of the spectrum of primordial scalar perturbations n_S and its running α_S . We set the spatial curvature outside the LTB patch, Ω_k , as well as the amplitude of primordial tensor perturbations to zero.

As discussed in Section 2.2, two additional parameters describe the LTB patch: the curvature at the center k_c and the comoving radius r_b . As shown in Table 1, we will use as actual parameters the present-day total density contrast and the present-day proper size of the radius, respectively. The latter is given by

$$d(r_b) \equiv \int_0^{r_b} \frac{Y'(r, t_0)}{\sqrt{1 - k(r)r^2}} dr, \quad (23)$$

and we define the former as

$$\delta_0 \equiv \frac{\rho_{\text{in}} - \rho_{\text{out}}}{\max(\rho_{\text{in}}, \rho_{\text{out}})}, \quad (24)$$

where $\rho_{\text{in}} = \rho_M(0, t_0) + \rho_X(0, t_0)$ and $\rho_{\text{out}} = \rho_{M, \text{out}}(t_0) + \rho_{X, \text{out}}(t_0)$. We calculate the contrast using the total density as in principle the dark-energy component can be as inhomogeneous as the matter component, and δ_0 should be a relevant physical quantity to be used. We chose a somewhat unusual definition by using $\max(\rho_{\text{in}}, \rho_{\text{out}})$ in the denominator. With this definition, this quantity fundamen-

tally satisfies $-1 < \delta_0 < 1$, such that the parameter-space volume in over- and under-densities is equally distributed. With the more usual definition we would have had $-1 < \frac{\rho_{\text{in}} - \rho_{\text{out}}}{\rho_{\text{out}}} < \infty$, which in the Bayesian parameter estimation induces a strong prior favouring large over-densities, possibly excluding under-densities from the analysis. In practice, however, the preferred values for this parameter are small, such that the difference between both definitions is almost negligible.

We discuss the priors in more detail in Appendix A. In the next section, where we discuss the results of the MCMC parameter estimation, we explore the full parameter space, never fixing the background parameters to some central value. Therefore we can always marginalize over all parameters, and do not bias the result in any way. That is, any possible degeneracy, expected or unexpected, between the cosmological parameters and the LTB parameters will show up and will not influence the results without being noticed.

4 RESULTS

The four left panes in Figure 2 show the parameters on which the main focus in this paper lies. This figure shows the two-dimensional marginalized posterior probability distributions of the background dark-energy density Ω_X , the dark-energy equation of state w_{out} , the boundary of the inhomogeneity in redshift space z_b , and the total density contrast in the inhomogeneity δ_0 (see Eq. (24)). Alternatively, in the four right panes of Figure 2 we use as proxies for z_b and δ_0 the apparent size that the inhomogeneity would subtend if located at the last scattering surface and its corresponding temperature anisotropy, respectively. Here we define the temperature perturbation $\Delta T/T$ as the relative difference in CMB temperature at the center of the inhomogeneity and outside, in the homogeneous (average) background. This is not necessarily representative for the average temperature in the spot.

The most interesting result is the clear degeneracy between δ_0 and w_{out} in the lower right pane in the left of Figure 2, and the degeneracy between δ_0 and Ω_X in the upper right pane. This graph explicates the necessity of properly modeling the inhomogeneity of the local universe, before any conclusion can be drawn on the properties of dark energy, in particular about the fundamental value of its equation of state: if the local density is ignored, the value of w_{out} can be misestimated by possibly 50%. Note also that the redshift up to which the inhomogeneity extends, z_b , is hardly of any influence on the central value of w_{out} or Ω_X . The bias on the parameters is indeed of opposite sign for opposite δ_0 . Therefore, as we marginalize over δ_0 in the combined posterior of w_{out} and z_b (lower left pane in Fig. 2), the total effect is compensated (we will come back to this point with Figure 3). Note, however, that the scatter does increase with the size of the inhomogeneity. The right of Figure 2 shows the dimensions that the inhomogeneity would have on the observed CMB temperature map, if it were centered on the observer's surface of last scattering. In this situation there are hence two identical inhomogeneities in the universe: one surrounding the observer, one centered on the observer's surface of last scattering. This figure shows that even spots that do

not violate the observables of Section 3, do induce a strong bias on w_{out} , following the findings of [Valkenburg \(2012b\)](#). As before we see that the apparent size of the inhomogeneity has almost no effect on the value of w_{out} or Ω_X .

In Figure 3 we show the one-dimensional marginalized posterior probabilities for Ω_X and w_{out} , under different priors on δ_0 , imposed by means of importance sampling on the MCMC chains that explore the full range of δ_0 . The result is displayed in black, and for comparison the constraints on these parameters for the homogeneous $w\text{CDM}$ model ($z_b \equiv 0$, $\delta_0 \equiv 0$) are displayed in dashed red lines. The top row shows Ω_X and w_{out} marginalized over all values of δ_0 , both positive and negative. Since positive and negative values of δ_0 have opposing effects on w_{out} and Ω_X , marginalizing over δ_0 mostly widens the tails of the distributions. This is already an important result showing how inhomogeneities contribute to the error budget in the cosmological parameters. This uncertainty from large-scale structures is expected to become more important when future data will tighten the confidence regions of the parameters of interest. If we impose, however, the prior that $\delta_0 > 0$ (second row in Figure 3) or $\delta_0 < 0$ (third row from top), we find even stronger results: we see indeed that both the tails and the central values of Ω_X and w_{out} shift. This shift is significant if one wants to progress towards not just precision but also accurate cosmology. If we push the magnitude even further, pretending we know that the local density must be either $\delta_0 = 0.1$ or $\delta_0 = -0.15$, as in the bottom row in Figure 3, then we find that $w = -1$ is excluded at 95% confidence level (c.l.) in both cases: $w < -1.03$ and $w > -0.98$, respectively. However, these particular models are only included at 99.7% c.l.

In order to better show the degeneracy of Ω_X and w_{out} with δ_0 we plot again in Figure 4 the corresponding two-dimensional marginalized posterior probabilities with 68%, 95%, 99.7% and 99.99% confidence level contours. Also plotted for comparison are the 95% c.l. one-dimensional constraints on Ω_X and w_{out} for the standard $w\text{CDM}$ model. This plot is meant to justify the values $\delta_0 = 0.1$ and $\delta_0 = -0.15$ used in the bottom row of Figure 3. It shows indeed that large values of $|\delta_0|$ that can significantly bias Ω_X and w_{out} are still within the 99.7% c.l.

4.1 Sensitivity to local Hubble-rate constraints

In Figure 5 we compare the effect of different Hubble-rate observations on the resulting posterior probabilities of Ω_X and w_{out} , when we fit the $w\text{CDM}$ model endowed with a local inhomogeneity to H_{loc} , SNe and CMB. As explained in Section 3.1, we compare the three different values from [Riess et al. \(2009\)](#) (solid black), [Freedman et al. \(2001\)](#) (dashed red) and [Sandage et al. \(2006\)](#) (dashed dotted blue). We see that the constraints on Ω_X do depend on the chosen measurement for H_{loc} , while the resulting constraints on w_{out} hardly depend on H_{loc} . This should be expected as SNe observations (constraining both Ω_X and w_{out}) are insensitive to H_{loc} while CMB observations (constraining Ω_X but weakly w_{out}) are instead sensitive to H_{loc} . These results imply that our conclusions with regard to w_{out} are robust against different observational determinations of H_{loc} , and the constraints hence mostly follow from the SNe and CMB.

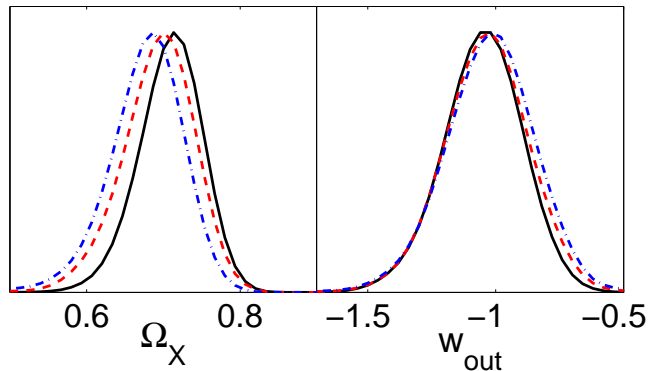


Figure 5. One-dimensional marginalized posterior probabilities of Ω_X and w_{out} for the inhomogeneous model, given CMB, SN and H_{loc} observations, comparing different constraints on H_{loc} : [Riess et al. \(2009\)](#) (solid black), [Freedman et al. \(2001\)](#) (dashed red) and [Sandage et al. \(2006\)](#) (dashed dotted blue). The conclusions about the effect of the inhomogeneity on w_{out} are robust against different observational determinations of H_{loc} .

4.2 kSZ effect

In Figure 6 we show the CMB dipole that observers at different radii would observe, for a given configuration; an overdensity on the left, an under-density on the right, in both cases the LTB patch has a radius of 1 Gpc, but with different values for w_{out} . Both cases fit the data roughly as well as the standard $w\text{CDM}$, while still giving an interesting bias on w_{out} .

We obtained these figures by – at each radius – starting an integration of the geodesic equations in two directions (negative and positive r -direction), back to the surface of last scattering, which lies at constant time in the synchronous gauge of the LTB metric. The difference in redshift to the surface of last scattering in both directions is then translated into a $\Delta T_{\text{CMB}}/T_{\text{CMB}} = (z_+ - z_-)/(2 + z_+ + z_-)$. Only for small radii this is to a good approximation equal to the dipole in a spherical harmonics expansion of the CMB temperature map. On the vertical axis on the righthand side we list the corresponding peculiar velocity that an observed temperature difference corresponds to, if it were the effect of peculiar velocity alone. For both panes, left and right, the peculiar velocities do not exceed the magnitude of expected random peculiar velocities. Therefore the kinematic Sunyaev-Zel’dovich effect that such velocities induce on CMB photons ([Garcia-Bellido & Haugboelle 2008](#); [Zhang & Stebbins 2011](#); [Zibin & Moss 2011](#)) should be at present undetectable. So as to strengthen this claim it is useful to look at the findings of [Valkenburg et al. \(2012\)](#) where constraints on the ALTB model from kSZ observations have been computed. While in the present paper dark energy is not the cosmological constant, the above analysis should give nevertheless an estimate of the kSZ signal. Therefore, this suggests that structures with a contrast of roughly ~ 0.1 extending for a radius of 1-2 Gpc are not excluded by present observations. A thorough study of the kSZ effect in these models is left to future work.

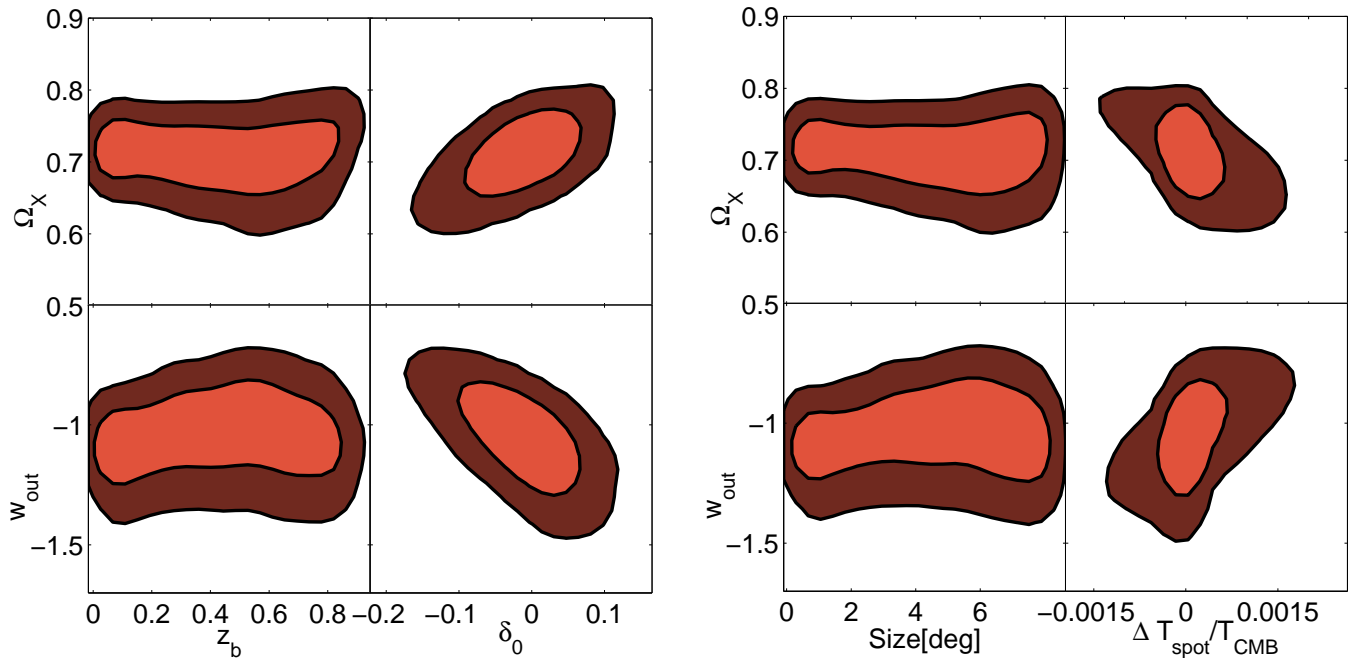


Figure 2. Two-dimensional marginalized posterior probability distributions for the most interesting parameters characterizing the w CDM model endowed with a local inhomogeneity considered in this paper. The parameters are constrained by the Union2 SN Compilation (Amanullah et al. 2010), the WMAP 7-year CMB power spectrum (Komatsu et al. 2011) and the recent determination of the Hubble rate by Riess et al. (2009). Inner tangerine-tango coloured contours are 68% confidence level (c.l.) contours, while the outer dark-red coloured contours are 95% c.l. The left and right figures show the same information, however the redshift of the boundary of the inhomogeneity, z_b , and the total density contrast, δ_0 , on the left, are on the right traded in for the angular diameter that the inhomogeneity would have if it were located at the observer’s last scattering surface and the temperature fluctuation that it would induce, respectively.

4.3 FLRW Observer’s $w(z)$

Following Clarkson et al. (2007) one can, given a luminosity distance-redshift relation in a homogeneous universe, compute what the underlying $w(z)$ of the dark-energy fluid is. In the homogeneous universe (described by the FLRW metric), one can find indeed an exact relation between $w(z)$ and the first and second derivatives of the luminosity distance with respect to redshift and two more parameters, Ω_k and Ω_m . If an observer knows the latter two parameters from other observations, and deduces the first and second derivatives of the luminosity distance from SN observations, the observer can derive $w(z)$. In the scenario studied here, at background level w is not a function of time or redshift. However, the inhomogeneity comes into play in the luminosity distance-redshift relation. Therefore, an observer that falsely assumes that the metric surrounding him/her is FLRW will in fact see a redshift dependence in w . We calculate the observed $w_{\text{obs}}(z)$ (Eq. (3) in Clarkson et al. 2007) for the two example models of Fig. 6, and show the result in Fig. 7. Inside the inhomogeneity, $w_{\text{obs}}(z)$ shows a very clear signature of the matter distribution: the contracting core and expanding compensating shell for the over-density show corresponding effects on $w_{\text{obs}}(z)$. The inverse holds for the under-density.

Therefore, if one performs an analysis such as in Shafieloo et al. (2009); Zhao et al. (2012), one may find a significant deviation from a constant w , while fundamentally w is constant at the background level. In particular, it is very interesting to note that the $w(z)$ reconstruction by Zhao et al. 2012 (see e.g. the pane (A2) of Fig. 1 in that

reference), if interpreted within this framework, could indicate the presence of a large-scale underdensity around us, and not of a possibly time-dependent equation of state. It is indeed worth noting the similarity of the result by Zhao et al. (2012) with the observed $w_{\text{obs}}(z)$ shown in Fig. 8, which corresponds to a Λ CDM model endowed with a local underdensity of central contrast $\delta_0 = -0.06$ and redshift boundary $z_b = 0.4$.

4.4 Other parameters

In Figure 9 we show posterior probabilities of H_0 , which is the expansion rate of the background universe (and does *not* correspond to the locally observed expansion rate), $\delta_0 \equiv \frac{\rho_{\text{in}} - \rho_{\text{out}}}{\max(\rho_{\text{in}}, \rho_{\text{out}})}$, $\delta_{M,0} \equiv \frac{\rho_{M,\text{in}}}{\rho_{M,\text{out}}} - 1$, and $\delta_{X,0} \equiv \frac{\rho_{X,\text{in}}}{\rho_{X,\text{out}}} - 1$. All other parameters that we allowed to vary, listed in Table 1, show practically no deviation in their constraints in the presence and absence of the inhomogeneity. The constraint on H_0 is significantly weakened when one takes into account the possibility that we may live in a local inhomogeneity. This result is similar to the findings in Valkenburg & Bjaelde (2012), even if the local inhomogeneity considered is orders of magnitude different. Moreover, the actual matter perturbation that is allowed by the data can be as large as $|\delta_{M,0}| \simeq 0.5$, leaving the total density perturbation around $|\delta_0| \simeq 0.1$, because the energy perturbation in the dark-energy fluid is generally small as w_{out} is never very far from -1.

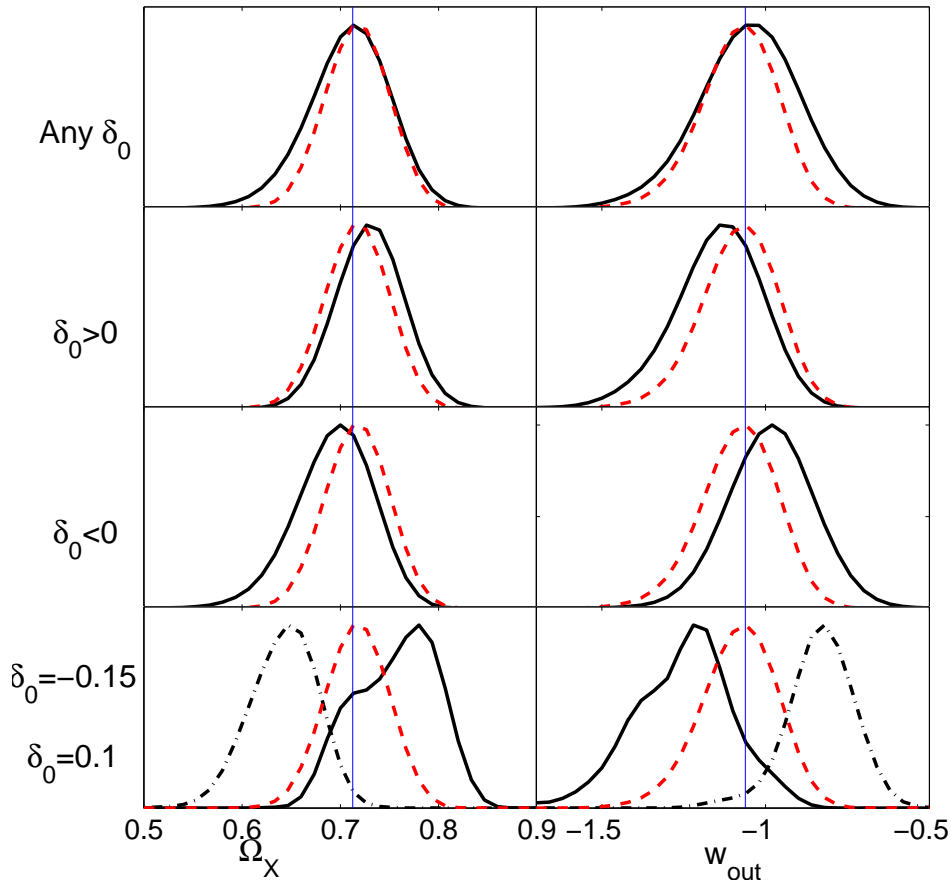


Figure 3. One-dimensional marginalized posterior probabilities for Ω_χ and w_{out} , constrained by CMB, SNe, and H_{loc} . The standard w CDM constraints on these parameters are shown in red dashed lines and are the same in the different panes. The blue vertical line serves as a guide for the eye, always going through the maximum of the w CDM value. The constraints on the w CDM model endowed with a local inhomogeneity considered in this paper are given under different priors on δ_0 : $-0.2 < \delta_0 < 0.2$ (top), $0 < \delta_0 < 0.2$ (second row from top), $-0.2 < \delta_0 < 0$ (third row from top), and for two constraining priors on δ_0 (bottom): $\delta_0 = 0.1$ (solid black line) and $\delta_0 = -0.15$ (dashed-dotted black line). A prior on δ_0 that averages around zero, widens but does not shift the posterior distributions. If we know instead the sign of δ_0 , constraints on w_{out} and Ω_χ shift by as much as 5% \sim 10%. In the bottom row, for $\delta_0 = 0.1$ the 95% c.l. upper bound on w_{out} is -1.03. For $\delta_0 = 0.15$ the 95% c.l. lower bound on w_{out} is -0.98. Both priors hence rule out the cosmological constant at 95% c.l., given current observations.

4.5 Probability under homogeneous initial conditions

Given the fact that we observe several large spots in the CMB, and the possibility that these spots are the result of density perturbations on the surface of last scattering, we can argue that living in such a perturbation must have a non-zero probability.⁵ If all perturbations arise from a smooth, close to scale invariant spectrum of primordial perturbations, it is not obvious that large cold and hot spots

⁵ We would like to point out that for the almost-linear models considered in this paper the observer does not need to be very close to the center so as not to see a too large CMB dipole. For the cases of Fig. 6, for example, the dipole is never larger than the observed value of $\sim 10^{-3}$. For larger contrasts there will be regions where observers would see a larger-than-measured dipole, but these regions will not occupy the majority of the inhomogeneity. Finally, we would like to stress that we have placed the observer at the center simply to simplify the numerical calculations.

should exist, and there is an ongoing debate about this topic (Cruz et al. 2006; Zhang & Huterer 2010; Ayaita et al. 2010).

Let us nonetheless quantify the probability of having the density perturbations that we took as examples for Figs. 6 and 7. If these perturbations come from the same spectrum as the perturbations that we observe in the CMB, then the probability of their existence can be approximated by the variance of the gaussian density field, smoothed by a top hat filter with a radius that corresponds to the radius of the density perturbation under consideration (Kolb & Turner 1990). It must be noted that, because of the compensated shape of the density profile that we consider, taking the full radius of the spherical patch, r_b , as the radius of the top hat filter would give almost zero density perturbation. Therefore we choose the radius at which the density changes sign as the smoothing radius. This is roughly at $r_b/2$, but we use the numerically obtained exact value. Comparing at the time of decoupling when dark energy is negligible, and with the primordial spectrum of perturbations of the two models respectively (since the models were

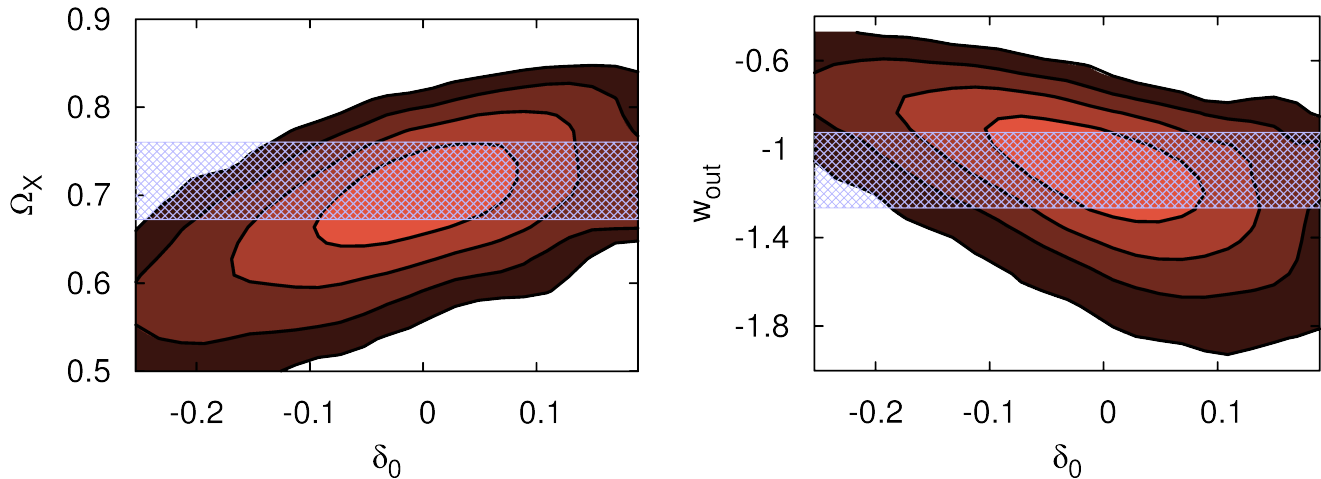


Figure 4. Two-dimensional marginalized posterior probabilities for Ω_X and w_{out} with δ_0 , constrained by CMB, SNe, and H_{loc} . The color shaded regions correspond from the innermost region to the outmost region to 68% c.l., 95% c.l., 99.7 % c.l. and 99.99% c.l., respectively. The blue horizontal band corresponds to the 95% c.l. one-dimensional constraints on Ω_X and w_{out} for the standard w CDM model. This plot shows that if future data will constrain $|\delta_0|$ to be large, then the inclusion of such data will shift the best fit region towards values of w that are far from -1 .

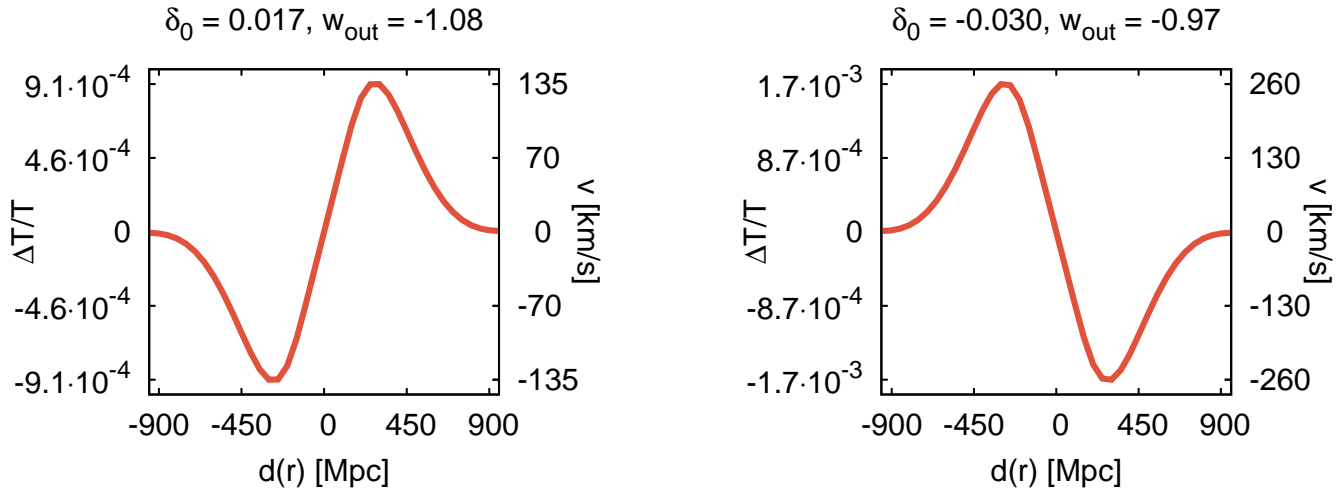


Figure 6. The CMB-dipole observed by observers at different radii $d(r)$ in an LTB patch with a radius of 1 Gpc, for an over-density (left) and an under-density (right). On the right vertical axis we list the corresponding peculiar velocity that is derived assuming that the observed CMB dipole is caused solely by the peculiar velocity of the observer. The magnitude of the velocities does not exceed the magnitude of expected random velocities. See Section 4.2 for more details.

fit to the CMB, they carry spectral parameters), we find that the over-dense model considered in Figs. 6 and 7 is at three times the dispersion of the smoothed density field of its cosmology (CMB spectrum), and the under-dense model is at six times the dispersion of its cosmology. Notably the over-dense model is not at all unlikely to occur, while it does give a large effect on both w_{out} and w_{obs} as shown in Fig. 7.

5 CONCLUSION

We have analyzed present observations of the local expansion rate, distant supernovae and the cosmic microwave background within a flat w CDM model endowed with a local almost-linear inhomogeneity surrounding the observer. We have found a significant impact on the dark-energy param-

eters, in particular on the equation of state which is strongly degenerate with the inhomogeneity contrast. The implications of this degeneracy are twofold. On one hand we have shown that with prior knowledge on the inhomogeneity, to be obtained possibly with some future probe, it is already possible to rule out the case of the cosmological constant with current data. On the other hand, even if future probes exclude the case of the cosmological constant in a homogeneous universe, this still may be due to a poor modeling of the large-scale structure of the universe. The same conclusions apply to constraints on the time variation of the equation of state.

The analysis in the present paper is but a first step towards a more accurate reconstruction of the cosmological parameters. We have indeed chosen, for technical reasons,

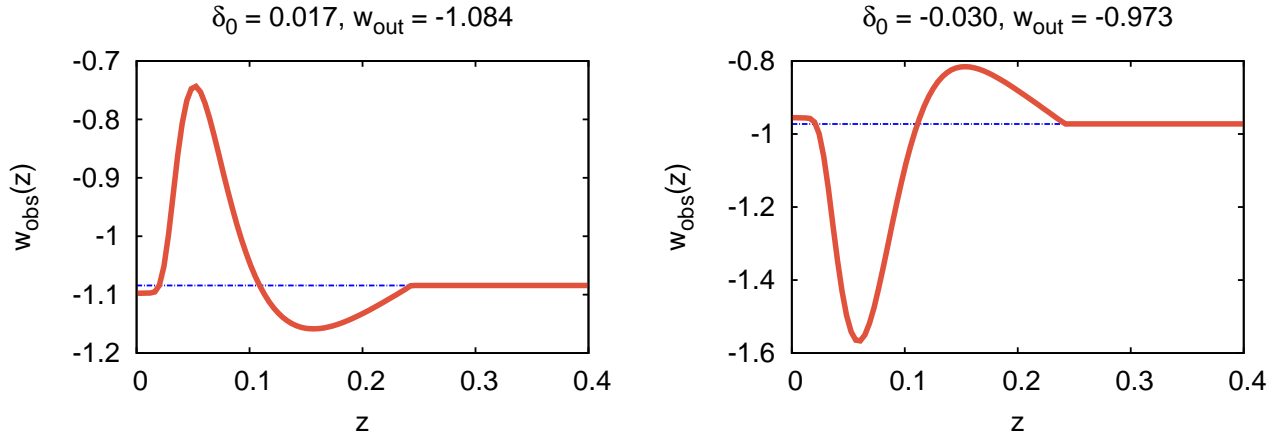


Figure 7. The function $w_{\text{obs}}(z)$ as defined in Clarkson et al. (2007), which is the equation of state of dark energy that an observer thinks to see if the observer falsely assumes that the universe is described by the FLRW metric. The examples shown here are the same two cosmologies as in Fig 6; an over-density (left) and an under-density (right). In both cases the observed $w_{\text{obs}}(z)$ (solid red) matches closely with the fundamental w_{out} (dashed blue) once the radius is reached where the spherically symmetric metric matches to the surrounding FLRW metric. The inhomogeneity causes clear features in $w_{\text{obs}}(z)$: the contracting core of the over-density increases the magnitude of $w_{\text{obs}}(z)$, while the under-dense compensating shell has the opposite effect. For the under-dense center, the inverse holds. In this picture $w_{\text{obs}}(z)$ is computed using the exact solutions, while taking second derivatives of observed distances would not necessarily reveal these features.

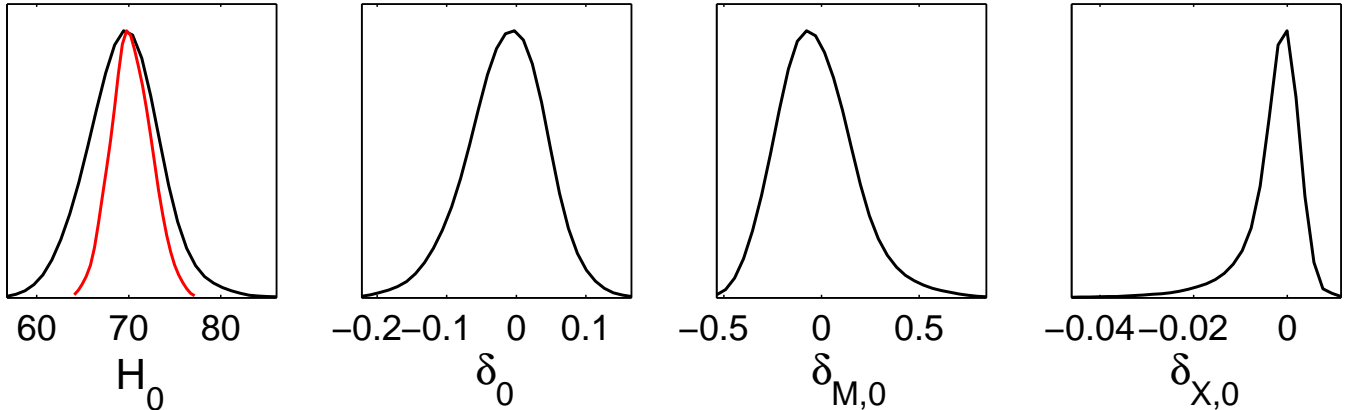


Figure 9. One-dimensional marginalized posterior probabilities of H_0 , which describes the age of the universe and does *not* correspond to the locally observed expansion rate, $\delta_0 \equiv \frac{\rho_{\text{in}} - \rho_{\text{out}}}{\max(\rho_{\text{in}}, \rho_{\text{out}})}$, $\delta_{M,0} \equiv \frac{\rho_{M,\text{in}}}{\rho_{M,\text{out}}} - 1$, and $\delta_{X,0} \equiv \frac{\rho_{X,\text{in}}}{\rho_{X,\text{out}}} - 1$. The presence of the spherical structure weakens significantly the bounds on the background expansion rate (in red we show the constraint on H_0 in the homogeneous $w\text{CDM}$ model). Secondly, the local energy perturbation consists of an almost negligible dark-energy perturbation and a significant dust perturbation, which is not apparent if one considers the total δ_0 alone.

a very specific dark-energy model and inhomogeneity profile. Before drawing definitive conclusions, a more comprehensive analysis should be performed. Firstly, it would be particularly interesting (even though perhaps challenging) to consider a nonzero dark-energy sound speed. However, since we found that the dark-energy component is only very mildly inhomogeneous, we do not expect our results to be strongly dependent on the assumption of a negligible sound speed. Secondly, it would be interesting to consider more inhomogeneous patches with more general density profiles, possibly with the observer at randomized positions (Marra et al. 2007, 2008; Valkenburg 2009; Szybká 2011; Flanagan et al. 2012).

ACKNOWLEDGMENTS

It is a pleasure to thank Luca Amendola and Ignacy Sawicki for useful comments and discussions. MP acknowledges financial support from the Magnus Ehrnrooth Foundation. VM and WV acknowledge funding from DFG through the project TRR33 “The Dark Universe”.

References

- Alonso D., Garcia-Bellido J., Haugbolle T., Vicente J., 2010, Phys.Rev., D82, 123530, [1010.3453](#)
Amanullah R., Lidman C., Rubin D., Aldering G., Astier P., et al., 2010, Astrophys.J., 716, 712, [1004.1711](#)

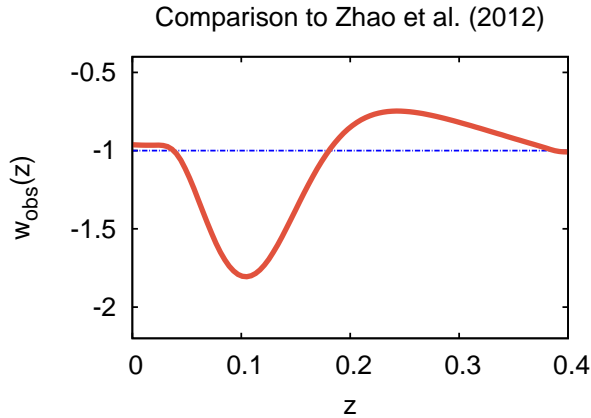


Figure 8. As in Fig. 7 but for a Λ CDM model endowed with a local underdensity of central contrast $\delta_0 = -0.06$ and redshift boundary $z_b = 0.4$ such that the observed $w_{\text{obs}}(z)$ appears qualitatively similar to the $w(z)$ reconstruction by Zhao et al. (2012) (see e.g. the pane (A2) of Fig. 1 in that reference). If interpreted within this framework, the results of Zhao et al. (2012) could indicate the presence of a large-scale underdensity around us, rather than a possibly time-dependent dark-energy equation of state.

Amendola L., Kainulainen K., Marra V., Quartin M., 2010, Phys.Rev.Lett., 105, 121302, [1002.1232](#)
 Ayaita Y., Weber M., Wetterich C., 2010, Phys.Rev., D81, 023507, [0905.3324](#)
 Ballesteros G., Lesgourgues J., 2010, JCAP, 1010, 014, [1004.5509](#)
 Bennett C. L., et al., 2011, ApJS, 192, 17, [1001.4758](#)
 Bertacca D., Bartolo N., Diaferio A., Matarrese S., 2008, JCAP, 0810, 023, [0807.1020](#)
 Bertacca D., Bartolo N., Matarrese S., 2010, Adv. Astron., 2010, 904379, [1008.0614](#)
 Biswas T., Notari A., Valkenburg W., 2010, JCAP, 1011, 030, [1007.3065](#)
 Clarkson C., Clifton T., February S., 2009, JCAP, 0906, 025, [0903.5040](#)
 Clarkson C., Cortes M., Bassett B. A., 2007, JCAP, 0708, 011, [astro-ph/0702670](#)
 Creminelli P., D'Amico G., Norena J., Vernizzi F., 2009, JCAP, 0902, 018, [0811.0827](#)
 Cruz M., Tucci M., Martinez-Gonzalez E., Vielva P., 2006, MNRAS, 369, 57, [astro-ph/0601427](#)
 de Lavallaz A., Fairbairn M., 2011, Phys.Rev., D84, 083005, [1106.1611](#)
 Deffayet C., Pujolas O., Sawicki I., Vikman A., 2010, JCAP, 1010, 026, [1008.0048](#)
 Enqvist K., Mattsson T., 2007, JCAP, 0702, 019, [astro-ph/0609120](#)
 Flanagan E. E., Kumar N., Wasserman I., Vanderveld R., 2012, Phys.Rev., D85, 023510, [1109.1873](#)
 Freedman W. L., et al., 2001, ApJ, 553, 47, [astro-ph/0012376](#)
 Garcia-Bellido J., Haugboelle T., 2008, JCAP, 0809, 016, [0807.1326](#)
 Inoue K. T., Silk J., 2006, ApJ, 648, 23, [astro-ph/0602478](#)
 Inoue K. T., Silk J., 2007, ApJ, 664, 650, [astro-ph/0612347](#)
 Kolb E. W., Turner M. S., 1990, Front.Phys., 69, 1

Komatsu E., et al., 2011, ApJS, 192, 18, [1001.4538](#)
 Lewis A., Bridle S., 2002, Phys. Rev., D66, 103511, [astro-ph/0205436](#)
 Lewis A., Challinor A., Lasenby A., 2000, ApJ, 538, 473, [astro-ph/9911177](#)
 Li M., Li X.-D., Wang S., Wang Y., 2011, Commun. Theor. Phys., 56, 525, [1103.5870](#)
 Lim E. A., Sawicki I., Vikman A., 2010, JCAP, 1005, 012, [1003.5751](#)
 Marra V., Kolb E. W., Matarrese S., 2008, Phys.Rev., D77, 023003, [0710.5505](#)
 Marra V., Kolb E. W., Matarrese S., Riotto A., 2007, Phys.Rev., D76, 123004, [0708.3622](#)
 Marra V., Notari A., 2011, Class.Quant.Grav., 28, 164004, [1102.1015](#)
 Marra V., Paakkonen M., 2010, JCAP, 1012, 021, [1009.4193](#)
 Marra V., Paakkonen M., 2012, JCAP, 1201, 025, [1105.6099](#)
 Masina I., Notari A., 2009, JCAP, 0902, 019, [0808.1811](#)
 Moss A., Zibin J. P., Scott D., 2011, Phys.Rev., D83, 103515, [1007.3725](#)
 Nishikawa R., Yoo C.-M., Nakao K.-i., 2012, Phys.Rev., D85, 103511, [1202.1582](#)
 Peebles P., 2002, [astro-ph/0208037](#)
 Perlmutter S., et al., 1999, Astrophys.J., 517, 565, [astro-ph/9812133](#)
 Riess A. G., et al., 1998, Astron.J., 116, 1009, [astro-ph/9805201](#)
 Riess A. G., et al., 2009, ApJ, 699, 539, [0905.0695](#)
 Romano A. E., Chen P., 2011, JCAP, 1110, 016, [1104.0730](#)
 Sandage A., et al., 2006, ApJ, 653, 843, [astro-ph/0603647](#)
 Shafieloo A., Sahni V., Starobinsky A. A., 2009, Phys.Rev., D80, 101301, [0903.5141](#)
 Sinclair B., Davis T. M., Haugbolle T., 2010, Astrophys.J., 718, 1445, [1006.0911](#)
 Szybkas S. J., 2011, Phys.Rev., D84, 044011, [1012.5239](#)
 Tomita K., 2005, Phys. Rev., D72, 103506, [astro-ph/0509518](#)
 Valkenburg W., 2009, JCAP, 0906, 010, [0902.4698](#)
 Valkenburg W., 2012a, Gen.Rel.Grav., 44, 2449, [1104.1082](#)
 Valkenburg W., 2012b, JCAP, 1201, 047, [1106.6042](#)
 Valkenburg W., Bjaelde O. E., 2012, Mon.Not.Roy.Astron.Soc., 424, 495, [1203.4567](#)
 Valkenburg W., Marra V., Clarkson C., 2012, [1209.4078](#)
 Van Acoleyen K., 2008, JCAP, 0810, 028, [0808.3554](#)
 Zhang P., Stebbins A., 2011, Phys.Rev.Lett., 107, 041301, [1009.3967](#)
 Zhang R., Huterer D., 2010, Astropart. Phys., 33, 69, [0908.3988](#)
 Zhao G.-B., Crittenden R. G., Pogosian L., Zhang X., 2012, Phys.Rev.Lett., 109, 171301, [1207.3804](#)
 Zibin J. P., 2008, Phys.Rev., D78, 043504, [0804.1787](#)
 Zibin J. P., 2011, Phys.Rev., D84, 123508, [1108.3068](#)
 Zibin J. P., Moss A., 2011, Class.Quant.Grav., 28, 164005, [1105.0909](#)
 Zumalacarregui M., Garcia-Bellido J., Ruiz-Lapuente P., 2012, JCAP, 1210, 009, [1201.2790](#)

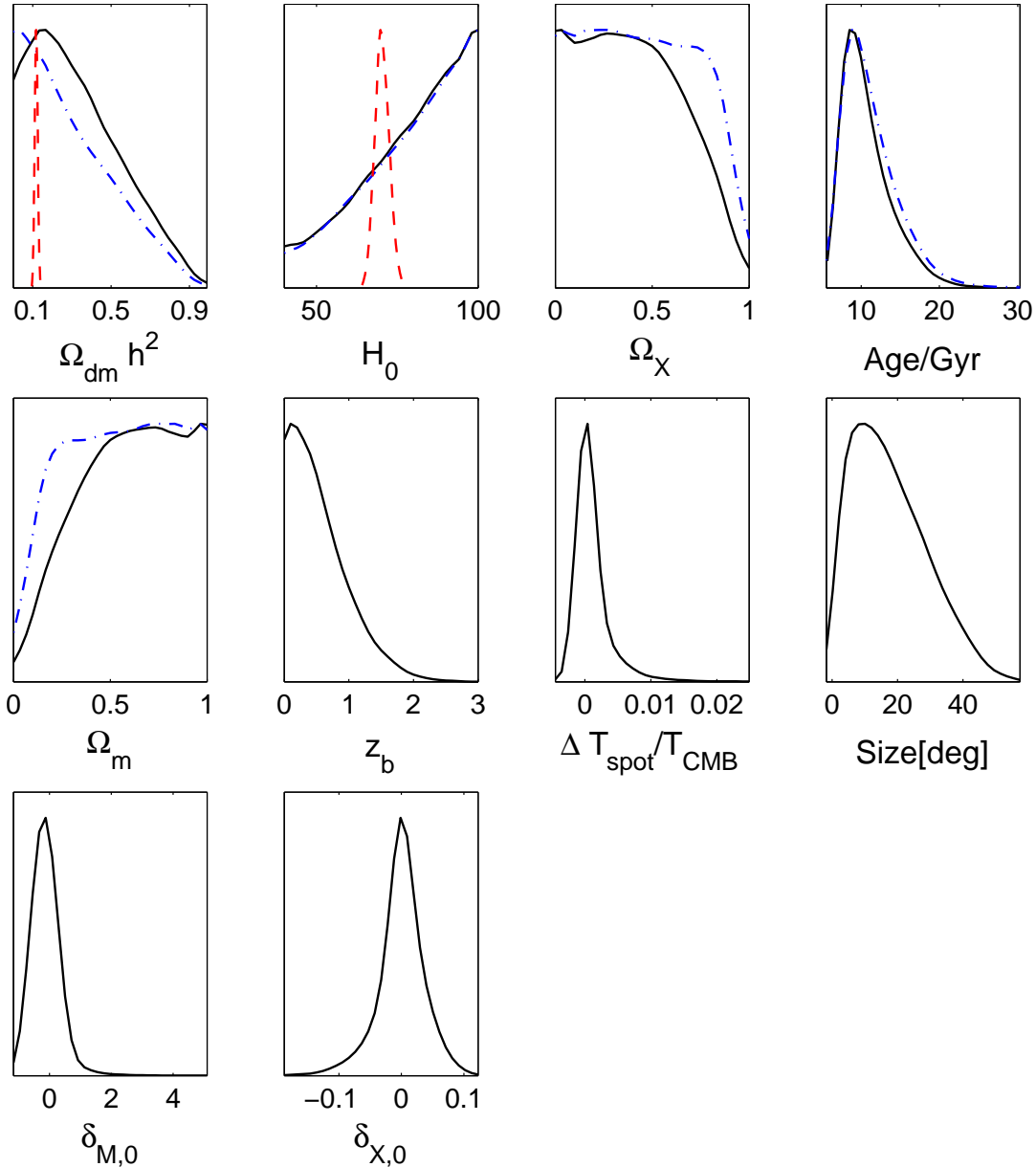


Figure A1. Priors on $\Omega_{\text{dm}}h^2$, H_0 and derived parameters, displaying those that are non-flat. The black (solid) lines represent the priors when the inhomogeneous metric is used, while the blue (dash-dot) lines represent the priors in the homogeneous w CDM case. For comparison, in red (dashed) we show the constraints on $\Omega_{\text{dm}}h^2$ and H_0 when the homogeneous w CDM case is fit to the data. The narrowness of the red curves shows that the data are very constraining on these parameters, and so the non-flat prior is of no importance. These prior distributions are obtained by running the MCMC analysis without any data, that is, accepting all points in parameter space with equal probability.

APPENDIX A: EFFECT OF CONSTRAINTS ON PRIORS

In Figure A1 we show the prior probability of $\Omega_{\text{dm}}h^2$, H_0 and derived parameters, since they dependent non-linearly on combinations of input parameters on which we take flat priors, and hence their prior probability is non-flat. We obtained these prior probabilities by running the MCMC analysis without any data, accepting all points in parameter space with equal probability. Maybe surprisingly, the actual prior probabilities on $\Omega_{\text{dm}}h^2$ and H_0 are not flat, even though we do list their prior ranges in Table 1 as flat, and

we indeed gave flat priors on these parameters in the input of the MCMC simulation. The non-flatness stems from the additional constraint $\Omega_X > 0$, demanding that the energy density of the dark-energy fluid is positive (if the Dark Energy is a pure cosmological constant nothing prevents $\Omega_\Lambda < 0$ from happening). Because we set $\Omega_k = 0$, this condition is satisfied only when $\Omega_m < 1$, or $\Omega_m h^2 < h^2$.

To explain the relation, let us simplify the priors to $0 < \Omega_m h^2 < 1$ and $0 < h < 1$. The starting point is a flat prior on these parameters, *i.e.* that the probability $P(\Omega_m h^2) = \text{constant}$ and $P(h) = \text{constant}$, normalized such

that $\int_0^1 P(x)dx = 1$ for x being both h and $\Omega_m h^2$. If we write shorthand notation C for the condition that $\Omega_X > 0$ and $\Omega_k = 0$, then imposing C we have the conditional joint probability,

$$P(\Omega_m h^2, h) \propto \begin{cases} P(\Omega_m h^2, h|C) = \text{constant} & \text{if } C \text{ is true} \\ 0 & \text{if } C \text{ is false} \end{cases}, \quad (\text{A1})$$

normalized such that

$$\int_0^1 \int_0^1 P(\Omega_m h^2, h|C) d(\Omega_m h^2) dh = 1. \quad (\text{A2})$$

Then we find for the probabilities of h and $\Omega_m h^2$, up to normalization constants,

$$\begin{aligned} P(h|C) &= \int_0^1 P(\Omega_m h^2, h|C) d(\Omega_m h^2) \\ &\propto \int_0^{h^2} d(\Omega_m h^2) \propto h^2, \end{aligned} \quad (\text{A3})$$

$$\begin{aligned} P(\Omega_m h^2|C) &= \int_0^1 P(\Omega_m h^2, h|C) dh \propto \int_{h=\sqrt{\Omega_m h^2}}^1 dh \\ &\propto 1 - \sqrt{\Omega_m h^2}, \end{aligned} \quad (\text{A4})$$

in agreement with the priors in Figure A1, favouring large h and small $\Omega_m h^2$. However, as can be seen from the red dashed curves in Figure A1, the data are constraining $\Omega_m h^2$ and H_0 so tightly, that the non-flatness of the prior has no effect on the final parameter estimation.

This paper has been typeset from a $\text{T}_{\text{E}}\text{X}/\text{L}^{\text{A}}\text{T}_{\text{E}}\text{X}$ file prepared by the author.